



# Uniaxial compressive strength measurements of limestone plugs and cores: a size comparison and X-ray CT study

Jeroen F. Van Stappen<sup>1,2</sup> · Tim De Kock<sup>1</sup> · Geert De Schutter<sup>3</sup> · Veerle Cnudde<sup>1</sup>

Received: 22 May 2018 / Accepted: 14 December 2018 / Published online: 6 January 2019  
© Springer-Verlag GmbH Germany, part of Springer Nature 2019

## Abstract

In many geo-engineering fields, the uniaxial compressive strength (UCS) of a rock material is the parameter most commonly used to define a rock's mechanical strength. Several international standards have been developed for determining this value, which require the tested material to have certain minimum dimensions and shapes. In many applications, however, sample material is limited. Therefore, this study investigates the possibility of determining the UCS on rock plugs smaller than the minimum dimensions in the most common standards. The materials investigated are four different depositional limestones from the Paris Basin which are often used as building material in France and Belgium. Results from UCS tests in a small-scale uniaxial compressive device are compared to standard-sized tests according to the governing international standards. The results show that the strength determined on the small-scale plugs is very similar to the UCS determined on standard-sized cores. Using high-resolution X-ray computed tomography, it was possible to investigate the failure modes of the small-scale plugs and link them to their internal rock fabric. Obtaining a three-dimensional visualization provides valuable insights into the origin of the variability in the UCS measurements in small-scale plugs.

**Keywords** Uniaxial compressive strength · High-resolution X-ray tomography · Building stones · Downsizing · Failure modes · Limestone

## Introduction

The uniaxial compressive strength (UCS) of a rock material is considered to be the most accurate and is the most commonly used parameter for determining a rock's mechanical strength. It depends not only on the rock's chemical and mineralogical

composition, but also strongly on its porosity, the rock's fabric, and the size and shape of the tested material (Siegesmund and Dürrast 2011; Ji et al. 2012; Liang et al. 2016). The UCS of rock material is one of the most important parameters in engineering applications, such as its use as armour stone or natural building material (Kahraman 2001; Benavente et al. 2004). Also, in reservoir applications, the mechanical strength of the reservoir rocks is used in order to understand the stability of the reservoir layers during drilling and production. Because of its importance in a broad range of geological fields, different international standards have been developed to determine a rock's UCS (Bieniawski and Bernede 1979; UNE-EN 1926 2007; ASTM C170/C170M-16 2016). These standards typically require the tested materials to have certain shapes (length-to-diameter ratio, or L:D ratio) and minimum dimensions. Table 1 summarizes the requirements for three of the most commonly used standards: the European standard for natural stones (UNE-EN 1926 2007), the American Society for Testing and Materials (ASTM) standard for determining compressive strength for dimension stones (C170/C170M-16 2016) and the method suggested by the International Society for Rock Mechanics (ISRM) for determining UCS (Bieniawski and Bernede 1979).

---

**Electronic supplementary material** The online version of this article (<https://doi.org/10.1007/s10064-018-01448-0>) contains supplementary material, which is available to authorized users.

---

✉ Jeroen F. Van Stappen  
j.f.vanstappen@uu.nl

- <sup>1</sup> PProGRess – UGCT, Department of Geology, Faculty of Sciences, Ghent University, Krijgslaan 281/S8, 9000 Ghent, Belgium
- <sup>2</sup> Present address: High Pressure and Temperature Laboratory, Department of Earth Sciences, Faculty of Geosciences, Utrecht University, P.O. Box 80.021, 3508TA Utrecht, The Netherlands
- <sup>3</sup> Magnel Laboratory for Concrete Research, Department of Structural Engineering, Faculty of Engineering and Architecture, Ghent University, Technologiepark Zwijnaarde 904, 9052 Ghent, Belgium

**Table 1** Different international standards developed for rock UCS testing and their requirements for sample shape and size

International standard	Shape of the sample	Minimum dimensions	L:D ratio
UNE-EN 1926	Cylindrical or cubic	D = 50 (± 5) mm or 70 (± 5) mm	1.0
ASTM	Cylindrical	D > 47 mm or 10 × largest grain	2.0–2.5
ISRM	Cylindrical	D > 54 mm or 10 × largest grain	2.5–3.0

Among the three most commonly used standards, the European standard stands out: it specifies that “Test specimens shall be cubes with (70 ± 5) mm or (50 ± 5) mm edges or right circular cylinders whose diameter and height are equal to (70 ± 5) mm or (50 ± 5) mm” (UNE-EN 1926 2007). This implies the use of an L:D ratio of 1, which differs from the ASTM and ISRM specifications. However, it is known that the shape of the tested material can have a significant effect on the outcome of the UCS measurements (Hoek and Brown 1980; Hawkins 1998; Tuncay and Hasancebi 2009; Siegesmund and Dürrast 2011). The current consensus is that an L:D ratio < 2 will result in (too) high UCS values, while an L:D ratio between 2 and 2.5 will yield only a slight difference in UCS measurements. If the L:D ratio is above 2.5, the UCS values will effectively remain constant (Thuro et al. 2001; Tuncay and Hasancebi 2009). In order to be able to compare UCS measurements obtained with different shapes, and thus L:D ratios, the ASTM proposes the following shape correction equation (Al-rkaby and Alafandi 2015; C170/C170M-16 2016):

$$UCS_{eq} = \frac{UCS_m}{0.778 + 0.222(l/d)^{-1}} \quad (1)$$

with  $UCS_{eq}$  the UCS of an equivalent rock with an L:D ratio of 1:1, and  $UCS_m$  the UCS value of a rock with a certain L:D ratio deviating from 1:1.

While there is relative consensus on the influence of the shape (L:D ratio) of a sample on UCS measurements, the influence of sample size can be put more to discussion. Two of the most important works in this field in fact contradict each other. Hoek and Brown (1980) reviewed literature data on UCS measurements performed on both cylindrical rock cores and cubic samples with dimensions between 10 and 200 mm. They found that the UCS decreased exponentially with increasing sample size. These data were based mostly on crystalline rock material, complemented with two sedimentary rocks. Hawkins (1998), on the other hand, focused on UCS measurements on sedimentary rock samples. Tests were performed on samples with diameters of between 12.5 and 150 mm. In this case, maximum rock strength values were obtained in the samples with diameters of 40–60 mm. Both below and above these dimensions, the obtained UCS values

were lower. Both studies, however, suggested that UCS measurements should be carried out on rock samples with a diameter of approximately 50 mm. This is, to date, the most commonly used size for the determination of the UCS, recommended by all three standards depicted in Table 1.

Generally, it is not desirable or possible to extract core samples with a diameter of 50 mm and a minimum L:D ratio of 2. For example, in reservoir engineering, sample material is often limited and highly valuable. Using sample dimensions smaller than the required 50 mm would logically reduce the total volume of sample material necessary for meaningful UCS measurements. In building restoration, the sampling of large cores for UCS testing is often omitted in order to avoid inflicting damage to the building or monument. In this study, the influence of sample size on the determination of the rock's UCS is investigated for four limestone types. The selected limestones are commonly used as building material in France and Belgium. The experiments were performed both on small-scale plugs with a diameter of approximately 10 mm and on standard-sized cores with a diameter of 45–50 mm. Using high-resolution X-ray computed tomography (micro-CT) (Cnudde and Boone 2013), three-dimensional images of the rock plugs were obtained prior to and after the UCS tests on the small rock plugs, which enabled the identification of the microstructural features controlling the failure of the rock.

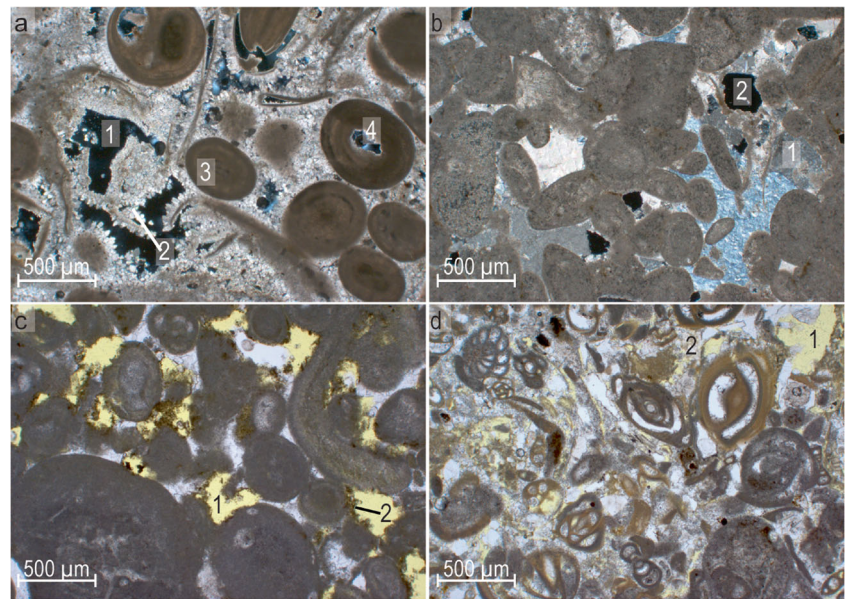
## Materials

Four depositional limestones were selected from the Paris Basin: the Savonnières, Massangis, Rocheville and Saint-Maximin limestones. They are mineralogically quite pure and differ from one another in their microstructure and pore size distribution. As such, different rock types could be tested, characterized by a broad range in porosity. Figure 1 shows thin-section images of the investigated limestones in which the different pore types are identified.

Savonnières limestone (Fig. 1a) is a monomineralic oolitic grainstone (Dunham 1962) (Late Jurassic, Tithonian), extracted in Savonnières-en-Perthois, France, from the Oolithe Vacuolaire stratigraphic unit. The pore structure in the rock consists of vacuolar ooids, connected by intra-oolitic micro-porosity to the intergranular micro- and macropores. The stone is further characterized by local layers of (dissolved) shell fragments, which add to the complexity of the rock's microstructure (Roels et al. 2001; Derluyn et al. 2014). The porosity of Savonnières limestone is known to range from 22 to 41%. The samples in this study have an open porosity between 29 and 35%.

Massangis limestone (Fig. 1b) is an oolitic packstone to grainstone (Dunham 1962) of the Oolithe Blanche Formation (Middle Jurassic, Bathonian), extracted in Massangis, France. Similar to the Savonnières limestone, it

**Fig. 1** Thin-section images of the investigated limestones: **a** Savonnières limestone, with intergranular macro- (1) and micropores (2) and intragranular micro- (3) and macropores (dissolved interior of ooids) (4); **b** Massangis limestone with intergranular micropores (1) due to the dissolution of micro-sparite, and moldic macropores (2) due to de-dolomitization; **c** Rocheville limestone with intergranular macro- (1) and micropores (2); **d** Saint-Maximin limestone with intergranular macro- (1) and micropores (2) and several partly dissolved bioclasts



consists almost entirely of  $\text{CaCO}_3$  (up to 98%). In addition to the ooids, which can be up to approximately 1 mm large, bioclasts are present in the form of crinoids, bryozoans, gastropods, mollusks and algae, among others. Massangis limestone is typically characterized by low porosity (13 to 14%), which is partly intergranular due to the dissolution of micro-sparite (micropores), and partly moldic (i.e. formed by selective removal of individual grains), related to de-dolomitization (macropores) (Makhloufi et al. 2013). The samples in this study have an open porosity ranging from 13.5 to 15.6%.

Rocheville limestone (Fig. 1c) (Middle Jurassic, Bathonian) is an oolitic packstone to wackestone (Dunham 1962), extracted in Villaines-en-Duesmois, France. The bioclasts are rather large and partly micritized. Their origin is diverse (e.g. gastropods, lamellibranches, algae, foraminifera, crinoids). Rocheville limestone has typical porosity ranging from 20 to 25%, which is intergranular and dominantly related to de-dolomitization. The samples investigated in this work are characterized by open porosities between 17.5 and 26.9%.

Saint-Maximin limestone (Fig. 1d) is a miliolid limestone from the Calcaire Grossier (Eocene, Lutetian) in the North of the Paris Basin (Fronteau et al. 2010). In this study, the Roche Franche Construction variety was used, which is characterized by a pore structure dominated by the dissolution of bioclasts. It has typical porosity ranging from 25 to 35%. The samples reported in this work have an open porosity between 23.5 and 26.1%.

## Experimental procedure

In this study, six rock cores of each of the limestone types, with a length and diameter of 89–91 mm and 45–45.6 mm, respectively, were obtained from larger blocks sampled in

the quarries in which the building materials are mined. The size of the rock cores deviates slightly from the recommended dimensions in the different international standards. This is due to the specific drill bits used to obtain the core samples. However, for all cores, an L:D ratio of 2:1 was used. All core samples were obtained perpendicular to the bedding of the rock samples, as described in UNE-EN 1926 (2007). To ensure flat and parallel end surfaces, the samples were finished on a surface grinder. The open porosity of the core samples was determined according to the vacuum-assisted water absorption test (UNE-EN 1936 2006), after which they were dried until constant mass and subjected to uniaxial compression on an MFL 6000-kN closed-loop compressive testing machine at the Magnel Laboratory for Concrete Research at Ghent University. After each test, the bearing surfaces of the testing machine were wiped clean and the next specimen was aligned to the center of the machine surfaces.

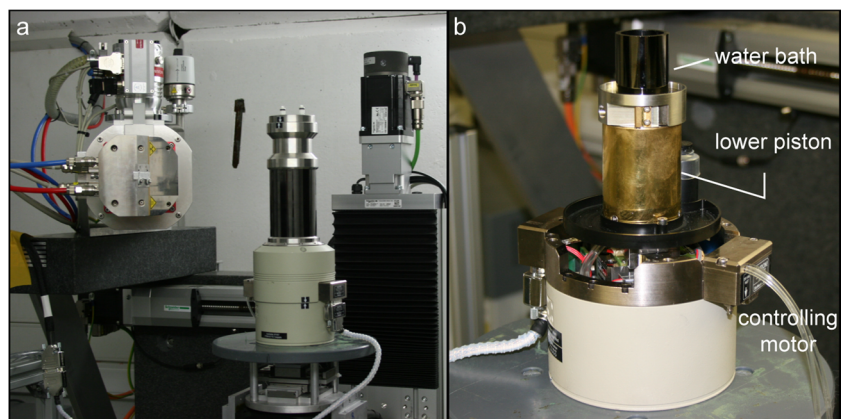
When possible, the same blocks were used in order to obtain small plugs, with length and diameter of 17–19 mm and 8–9 mm, respectively. For each of the limestone types, ten small-scale plugs were obtained. As with the larger core samples, the plugs were obtained perpendicular to the bedding of the rock material. To ensure parallel and flat surfaces, the samples were manually ground using 3D printed fittings. Their open porosity was determined with the vacuum-assisted water absorption test. The samples were dried until constant mass and their UCS was determined using a small-scale uniaxial compression device, the CT5000-TEC, developed by Deben Ltd., UK. This device was specifically adjusted to fit on the micro-CT systems at the Centre for X-ray Tomography at Ghent University (UGCT) (Masschaele



et al. 2007; Dierick et al. 2014). It allows small rock plugs to be subjected to uniaxial compression, with a maximum force of 5000 N. During the UCS experiments, the CT5000-TEC system was controlled using Deben Microtest software. Because compression with a constant stress rate was not possible, a constant strain rate of 0.1 mm/min was used during the UCS measurements. After each test, the two end caps of the CT5000-TEC device were wiped clean and loose grit was removed. Figure 2 shows the device as it was mounted on the sample stage of HECTOR, one of the micro-CT systems at UGCT. In both cases (larger specimens tested with the MFL 6000 and smaller specimens with the CT5000-TEC device), the stiffness of the testing device is known to be significantly higher than the stiffness of the test specimens. Potential effects of different stiffness of the testing devices on the obtained strength results can therefore be neglected.

For eight of the 40 investigated rock plugs, micro-CT scans were taken prior to and after reaching the peak stress in the UCS measurement. Micro-CT imaging is based on the attenuation of X-rays when they pass through matter. It allows the 3D visualization and quantification of the rocks' microstructure before and after rock failure. In this study, all micro-CT scans were carried out on the HECTOR system at UGCT (Masschaele et al. 2007). This scanner is equipped with an XWT 240-SE microfocus X-ray source and a large PerkinElmer flat panel detector. In combination with the CT5000-TEC device, micro-CT images can be obtained with a maximum spatial resolution of 10  $\mu\text{m}$ . However, the experiments described in this paper allowed the detector to be used in the  $2 \times 2$  binning mode, resulting in a spatial resolution slightly higher than 20  $\mu\text{m}$ . The micro-CT scans were performed by taking 1400 projection images with an exposure time of 1000 ms/projection. The X-ray source accelerating voltage was 140 kV and the output power was 22 W. A 1-mm-thick aluminum hardware filter was used to reduce the beam-hardening effect.

**Fig. 2** The Deben CT5000-TEC device as mounted on the HECTOR sample stage (a), and a detail of the lower part of the compression cell (b), with a water bath on top, allowing the samples to be tested in wet conditions if necessary



## Empirical relations: UCS versus porosity

Various studies have related the UCS of sedimentary rock material to other physical properties of samples. These studies were compiled and discussed by Chang et al. (2006). For limestones, they reported three formulas which relate the UCS to the rocks' porosity:

$$UCS = 276 \cdot (1 - 3\phi)^2 \quad (2)$$

$$UCS = 143,8 \exp(-6,95\phi) \quad (3)$$

$$UCS = 135,9 \exp(-4,85\phi) \quad (4)$$

with  $UCS$  the uniaxial compressive strength of the rock (MPa), and  $\phi$  the sample's total porosity (%). Equation 2 is said to define an upper bound of the UCS for a given porosity  $\phi$  and is considered to be favorable only for limestones with moderate porosities between 10 and 20%. Equations 3 and 4, on the other hand, give an estimate of the average rock strength for a given porosity. According to Chang et al. (2006), these equations tend to fit the data quite well for limestones with low to moderate porosity (< 20%) and relatively high UCS (> 30 MPa and > 10 MPa for Eqs. 3 and 4, respectively). It must be noted that Eqs. 2–4 link the UCS to the total porosity of the sample, while in this work, the porosity of the samples was determined according to the European standard UNE-EN 1936 (2006), which determines the open porosity of rock samples. However, for the limestones which were used, it is known that the open porosity can substitute for the total porosity, since there are few to no closed pores present within these stones.

## Results and discussion

### UCS

The samples had a nominal L:D ratio of 2:1. Minor deviations from this nominal value ranged from 1.97 to 2.01 for the

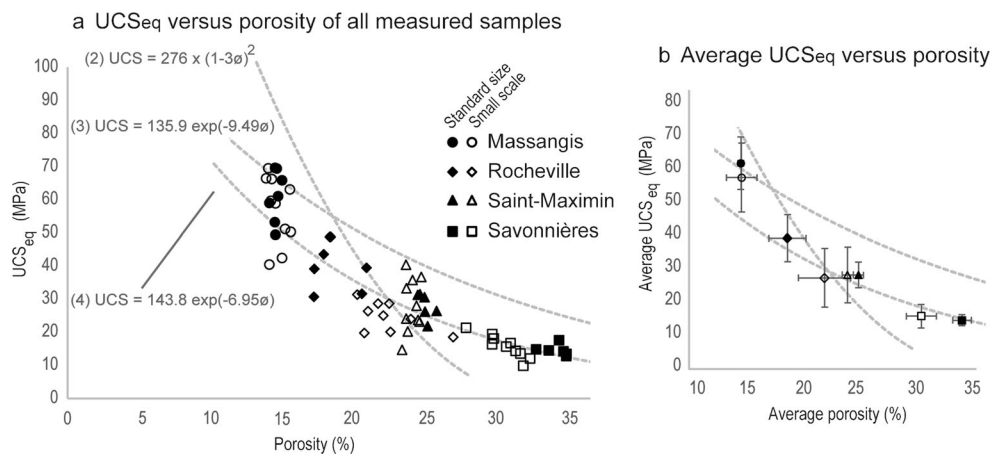
standard-sized samples and from 2.00 to 2.22 for the small-scale plugs. In order to compare the UCS values obtained in the standard size and small size setup, and thus isolate the size effect in the measurements, all UCS measurements were corrected using the shape-correction factor described in Eq. 1. The UCS values depicted in Fig. 3 are thus all  $UCS_{eq}$  values. If a size effect is present in the original, uncorrected UCS values, this is believed to be unaffected by the shape correction (Al-rkaby and Alafandi 2015; C170/C170M-16 2016). Comparing the  $UCS_{eq}$  values, hence, allows the measurements on small-scale plug and standard-sized core samples to be evaluated for differences related to sample size. Because of the significant range in porosity between the different limestones, Eqs. 2, 3 and 4 can be evaluated for their accuracy with regard to these particular rock types. To complement Fig. 3, the [Electronic Supplementary Material](#) includes a table in which the porosity, L:D ratio and  $UCS_{eq}$  value of each of the investigated samples is given.

Figure 3a shows that the  $UCS_{eq}$  values decrease exponentially when the porosity of the rock material increases. Equation 2 therefore does not fit the natural distribution of rock strength when compared with its porosity. Both Eqs. 3 and 4, however, follow the natural distribution of the experimental  $UCS_{eq}$  values. Equation 3 provides an upper limit for most of the measurements, while Eq. 4 tends to fit both standard-sized and small-scale plug measurements. The experimental data were fitted to this latter equation in Matlab in order to determine an  $R^2$  value for the fit. For the standard-sized samples, the equation fits with an  $R^2$  value of 0.84. For the small-scale plugs, the  $R^2$  value is 0.81. The Savonnières samples, characterized by a high porosity (> 29%) and a  $UCS_{eq}$  between 10 and 20 MPa, fit the equation particularly well. For the Massangis and Saint-Maximin samples, a larger spread in the  $UCS_{eq}$  is observed relative to their small spread

in porosity. This also is observed in Fig. 3b, where the mean porosity is plotted against the mean  $UCS_{eq}$  value, both with their standard deviation added as error bars. Table 2 also presents the mean values of the porosity and  $UCS_{eq}$  measurements, together with their standard deviations.

When comparing the  $UCS_{eq}$  of the core- and plug-sized samples, one has to consider the spread in porosity of the samples. To this end, Fig. 3b clearly illustrates that if the porosity of the samples is comparable (which is the case for the Massangis and Saint-Maximin limestones), there is no significant difference in the  $UCS_{eq}$  values obtained on core- and plug-sized samples. A one-on-one comparison for the Rocheville and Savonnières samples is hampered by the spread in porosity between the core- and plug-sized samples. However, all samples can be approached by equations described in the literature (Chang et al. 2006), which strengthens the belief that there is also no significant difference between the  $UCS_{eq}$  measured on core- and plug-sized samples for the Rocheville and Savonnières limestones. This seems to contradict both Hoek and Brown (1980) and Hawkins (1998). While most studies have confirmed the findings of Hoek and Brown (1980) that rock strength decreases with increasing sample diameter above 50 mm (Bieniawski and Bernede 1979; Hawkins 1998; Al-rkaby and Alafandi 2015), few have focused on testing sedimentary rocks with a diameter smaller than 50 mm. For the tested limestones in this study, it seems there is no size effect present when comparing samples with the same shape (cylindrical, with an L:D ratio of 2.0) but different sizes (small plugs with a diameter < 10 mm vs. standard cores with a diameter of 45–50 mm).

The decrease in rock strength with increasing sample size is often attributed to the presence of local zones of weakness along which fractures are induced. With an increase in sample size, the probability that such zones are present within the



**Fig. 3** a  $UCS_{eq}$  (Mpa) of limestones as a function of their porosity (%). The measurements of the Massangis, Rocheville, Saint-Maximin and Savonnières limestones are represented by circles, tilted squares, triangles and squares, respectively. The standard-sized measurements are shown as filled symbols, while the measurements on small-scale plugs are hollow.

Empirical literature trend lines 2, 3 and 4 are represented by dotted lines. b The mean  $UCS_{eq}$  (MPa) compared to the mean porosity (%) for each limestone type (small-scale plugs compared to standard-sized samples), with their standard deviation presented as error bars

**Table 2** Mean porosity and UCS<sub>eq</sub> values, together with their standard deviation (SD), for each of the analyzed rock types (plug vs. core comparison)

Rock type	Mean porosity (%)	SD porosity (%)	Mean UCS <sub>eq</sub> (MPa)	SD UCS <sub>eq</sub> (MPa)
Massangis (small)	14.6	0.6	56.8	10.2
Massangis (large)	14.6	0.3	61.0	7.8
Rocheville (small)	22.0	2.3	27.0	8.7
Rocheville (large)	18.7	1.6	38.8	6.9
St-Maximin (small)	24.0	0.5	27.9	8.3
St-Maximin (large)	25.0	0.5	27.9	3.8
Savonnières (small)	30.6	1.3	15.7	3.5
Savonnières (large)	34.2	0.8	14.5	1.7

sample increases, and so the average measured strength decreases (Paterson and Wong 2005). Thus, to understand the failure of the material, one must identify the potential structures of weakness in the sample. Typically, these are pre-existing micro-cracks or alignments of weak minerals. Along these structures, micro-cracks develop, which align immediately before the failure of the sample (Lockner 1993; Eberhardt et al. 1999). Since there is little to no difference in the obtained UCS<sub>eq</sub> between the small-scale plugs and the standard-sized cores, the micro-CT images of the small-scale plugs taken before and after the UCS experiments can help in understanding how the microstructure of the sample affects the UCS measurements in both the small-scale experiments and the standard-sized cores.

### Micro-CT observations

Szwedzicki and Shamu (1999) investigated the effect of discontinuities on the strength and failure of rock samples. Prior to subjecting a rock sample to a UCS test, they detected microscopic flaws, such as micro-cracks or the presence of bedding planes, at the surface of rock samples with a fluorescent dye and optical microscopy, enabling them to link the failure of the sample to pre-existing discontinuities in the rock

sample. Four different failure modes were detected: simple shear, multiple shear, multiple fracture and vertical splitting. Figure 4 schematically represents these different types of failure. Identical modes of failure have been detected in volcanic and metamorphic rocks and in sandstones (Basu et al. 2013).

Simple shear is the failure of a sample along one or more planes (parallel to each other) at an oblique angle to the direction of maximum compression. Multiple shear is the failure along two or more planes oblique to the direction of maximum compression, but not parallel to each other (Szwedzicki and Shamu 1999). When a rock sample disintegrates along many planes in random directions, the failure occurs in the multiple fracture mode. When the fractures propagate parallel to the direction of maximum compression, failure of the sample occurs through vertical splitting. It was observed that the location, orientation and size of areas of weakness influence the failure mode of a sample (Szwedzicki and Shamu 1999). When such an area of weakness is located at the end sections of a sample, the sample will fail in simple shear or multiple shear mode, while samples with discontinuities in the middle of them tend to fail via multiple fracturing. Shear is linked to an oblique orientation of the discontinuities to the direction of the main load, while vertical splitting is linked to discontinuities parallel to the loading direction. The chance that a

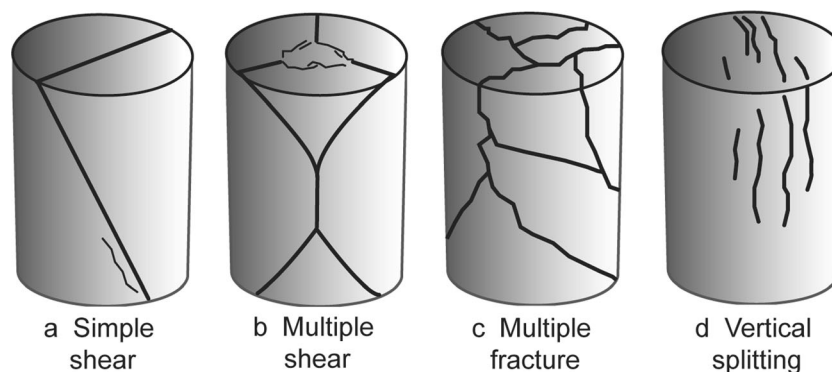


**Fig. 4** Failure modes in UCS tests: **a** simple shear; **b** multiple shear; **c** multiple fracture and **d** vertical splitting. Figure modified after Szwedzicki and Shamu (1999)



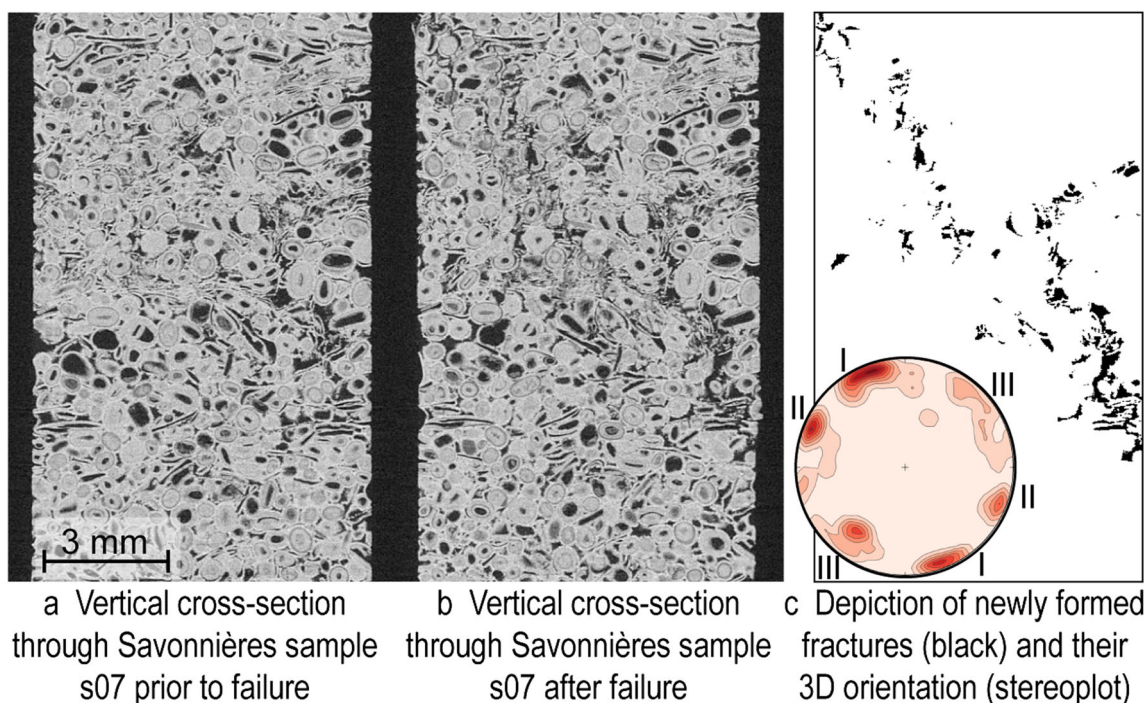
fracture will propagate through an area of weakness depends on the sample size and on the size of the zone of weakness relative to it. The macro-scale observations of the failure types are depicted in Fig. 4, and observed in both standard-sized samples as in the small-scale plugs, can thus be directly linked to the micro-scale fabric of the rock samples.

Figure 5 illustrates the micro-CT observations on a Savonnières plug with an initial open porosity of 29.7%. It shows a vertical slice through the sample before (Fig. 5a) and after failure (Fig. 5b). The resolution of the micro-CT images (23.4  $\mu\text{m}$ ) was too limited to resolve the connections between individual macropores in the micro-CT scan taken prior to failure of the plug. Segmenting these macropores based on their gray value would thus result in the definition of individual 3D objects within the micro-CT volume, representing the separate pores. After failure, a fracture is formed, which connects these individual macropores. It was possible to isolate the complete fracture, together with the original pores cut through by the fracture (Fig. 5c). A digital object separation step allowed the separation of the fracture into different smaller subsections. In each of these subsections, the orientation within the micro-CT scan could be determined. These orientations were plotted in a stereographical projection shown in Fig. 5c as a heat map of the poles to the fracture planes. These data were filtered for the most oblique fracture segments, showing

the presence of three separate fracture sets in this particular plug. In this way, the failure mode of the rock plug can be determined, in this case multiple shear.

Within the investigated Savonnières plugs, the fracture formation is strongly linked to the presence of local layers of dissolved shell fragments in between the ooids (Fig. 6a). These act as weak structures and allow the fracture to propagate along them. In the investigated plugs, these layers were present only in the upper half of the fracture. According to Szwedzicki and Shamu (1999), the samples should therefore fail in simple or multiple shear mode, which was confirmed through the micro-CT observations. In Fig. 5a and b, relative movement of the lower left half of the plug to the upper right part of the plug is observed: at the upper right part, the structures in Fig. 5a and b are identical, while the lower left part has shifted so that the structures in this vertical cross section are no longer identical. The three separate fracture sets detected in the Savonnières plug depicted in Fig. 5 indicate that this rock has failed by multiple shearing. The local layers with dissolved shell fragments allow the fracture to propagate through them. However, in the micro-CT images, the fracture is more pronounced in the areas where these layers are absent. The fracture width is greatest where the fracture had to break up individual ooids (Fig. 6a).

In the Saint-Maximin limestone samples, similar observations were made: in these samples, dissolved bioclasts acted as weak constituents of the rock matrix along which



**Fig. 5** **a** A vertical cross section through the micro-CT volume of one of the Savonnières samples prior to failure. **b** The same plug after failure, with a fracture from the top left to the middle right. **c** Pores affected by the

fracture (in black) and the orientation of the fracture as poles to the fracture planes, depicted in a stereoplot

the fracture propagated (Fig. 6b). Depending on their location and orientation within the plug, the samples failed under simple shear or vertical splitting conditions. The micro-CT image depicted in Fig. 6b shows a Saint-Maximin sample with an open porosity of 23.4% which failed under vertical splitting conditions. The fractures propagate along the fossils within the rock plug (amongst which miliolids and an elongated shell fragment occur). With regard to the strength measurements of the Saint-Maximin and Savonnières limestones, it must be noted that the Saint-Maximin limestones show more variability in strength than the Savonnières samples. This can be linked to the size of the constituent (fossil) grains within the samples. While the maximum size of an individual ooid in a Savonnières sample is limited to approximately 0.9 mm, the investigated Saint-Maximin plugs show the presence of (partly) dissolved bioclasts with length ranging from 2 to 6 mm (Fig. 6b). These bioclasts are thus larger than one-tenth of the diameter of the investigated plugs. These plugs therefore do not meet what is often stated as a second requirement for UCS measurements (Table 1: diameter of the investigated sample  $\geq 10$  times the largest grain). The large size of the dissolved bioclasts, compared to the diameter of the plug, can thus

be responsible for the variability in UCS measurements for a given porosity. This is supported by the fact that the standard-sized samples show less variability in their UCS values compared to the smaller samples (Fig. 3b). In the standard-sized samples, the diameter of the sample definitely exceeds the limit of 10 times the length of the largest grain.

In Rocheville and Massangis samples (Fig. 6c and d, respectively), the fracture propagation is influenced by strong structures rather than by weak structures. In both limestone types, the fractures propagate in the transition zone between large, elongated botryoidal calcite grains and smaller grains which appear darker in the micro-CT images. This is most obvious in the micro-CT images of the investigated Rocheville plugs. Because of the chemical purity of the rock samples, the darker grains in the micro-CT images indicate the presence of (micro-) pores which could not be resolved. The fractures propagate along the large botryoidal grains lacking the unresolved pores, which act as a strong structure. In the Rocheville plugs, these grains are clearly elongated and can measure up to 3.5 mm in length. These structures could potentially influence the UCS measurements of the plugs in a similar manner as the dissolved bioclasts in the Saint-Maximin plugs. The size of the

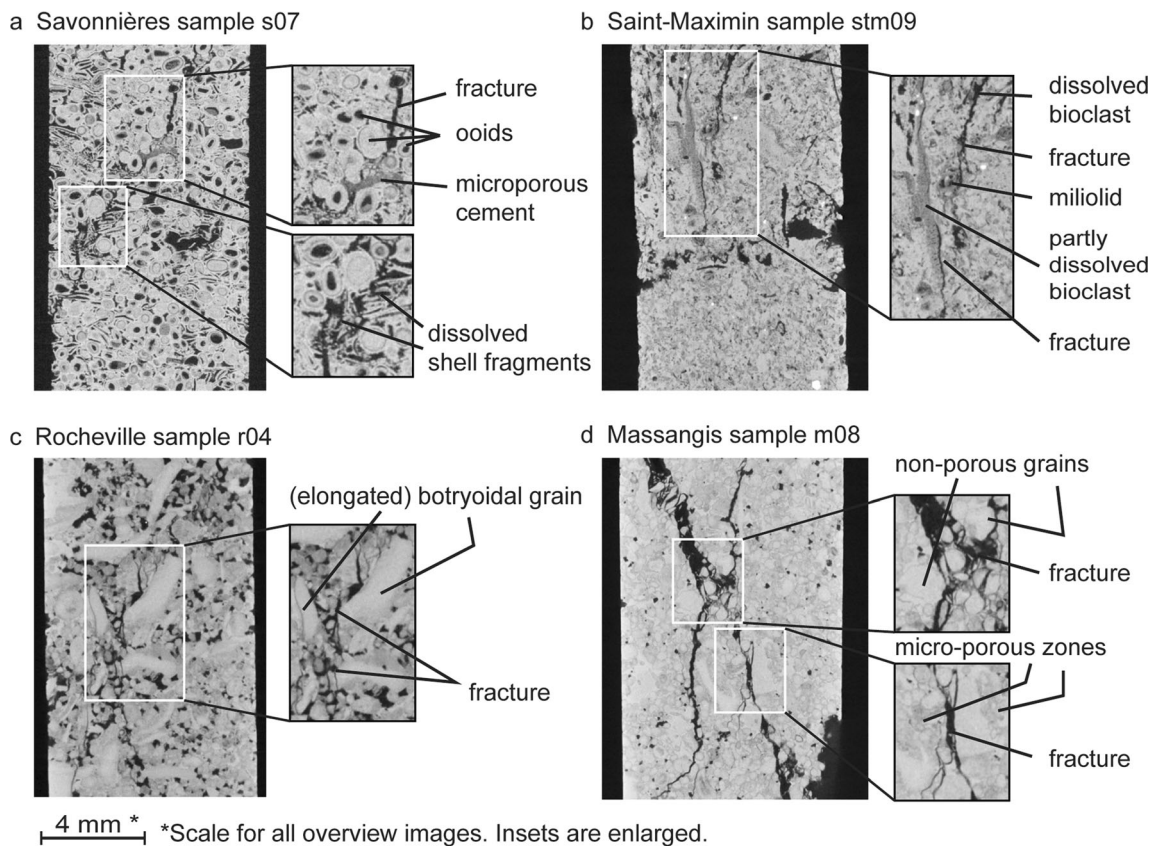


**Fig. 6** Micro-CT images after failure of the samples and the controlling structures for fracture formation of the Savonnières plug (a), the Saint-Maximin plug (b), the Rocheville plug (c) and the Massangis plug (d)



the botryoidal grains could explain the rather large spread in UCS measurements of the Rocheville and Massangis samples depicted in Fig. 3, as in the Saint-Maximin samples. The largest grains in both limestone types, as investigated with micro-CT, are found to be approximately 3.5 mm. Assuming similar grain size distributions, the UCS measurements in standard-sized samples are expected to show less variability for a given porosity range. In Fig. 3, this seems to be partly true. However, the standard-sized Massangis samples in particular still show large variability in UCS values. This could be related to the spatial distribution of the stronger botryoidal calcite grains within the investigated samples. Because only two of ten Massangis plugs were imaged, however, no real conclusions can be drawn regarding the role of the 3D distribution of strong particles. This is especially true because the two samples for which micro-CT images were obtained were characterized by similar porosities and  $UCS_{eq}$  values (13.9% and 66.4 MPa vs. 14.2% and 59.6 MPa), compared to the spread present in Fig. 3 ( $UCS_{eq}$  values ranging from 40 to 70 MPa).

## Conclusions

In this work we have compared UCS measurements on standard-sized limestone cores to measurements on small-scale plugs with a diameter of approximately 10 mm and an L:D ratio of 2:1. The measurements on the small-scale plugs were conducted using a commercial compression device produced by Deben Ltd., UK. Although this device only allows control of the displacement rate, and not the stress rate (as required by the international standards), the UCS measurements have been shown to be reliable, and comparable to standard-sized measurements for the materials used, depositional limestones. In addition, the downscaling allowed the use of high-resolution X-ray CT to study the fracture pattern and understand the mode of failure as a function of rock fabric. This allowed us to investigate the variability in the UCS measurements obtained on the small-scale plugs. Variability in the UCS obtained on small-scale plugs is believed to be linked to the presence and distribution of grains larger than one-tenth of the diameter of the investigated plug. However, in the investigated depositional limestones, similar variability is found in UCS measurements conducted on standard-sized samples. This might be linked to heterogeneity at the scale of the core.

**Acknowledgements** The Special Research Fund (BOF) at Ghent University is acknowledged for the finalizing PhD grant 01DI1316 for Jeroen Van Stappen. Tim De Kock is a postdoctoral fellow of the Research Foundation – Flanders (FWO) and acknowledges its support. FWO is also acknowledged for funding project G.0041.15 N which allowed the purchase of the uniaxial compressive device. For this, the Faculty Commission for Scientific Research (FCWO) at Ghent University is also acknowledged for its support.

## References

- Al-rkaby AHJ, Alafandi ZMS (2015) Size effect on the unconfined compressive strength and Modulus of elasticity of limestone rock. *Electron J Geotech Eng* 20:5143–5149
- ASTM C170/C170M-16 (2016) Standard test method for compressive strength of dimension stone. In: Book of ASTM standards, volume 04.07. West Conshohocken, PA
- Basu A, Mishra DA, Roychowdhury K (2013) Rock failure modes under uniaxial compression, Brazilian, and point load tests. *Bull Eng Geol Environ* 72:457–475. <https://doi.org/10.1007/s10064-013-0505-4>
- Benavente D, Garcia del Cura MA, Fort R, Ordóñez S (2004) Durability estimation of porous building stones from pore structure and strength. *Eng Geol* 74:113–127. <https://doi.org/10.1016/J.ENGEO.2004.03.005>
- Bieniawski ZT, Bernede MJ (1979) Suggested methods for determining the uniaxial compressive strength and deformability of rock materials. *Int J Rock Mech Min Sci Geomech Abstr* 16:137. [https://doi.org/10.1016/0148-9062\(79\)91450-5](https://doi.org/10.1016/0148-9062(79)91450-5)
- C170/C170M-16 (2016) Standard test method for compressive strength of dimension stone. West Conshohocken, PA
- Chang C, Zoback MD, Khaksar A (2006) Empirical relations between rock strength and physical properties in sedimentary rocks. *J Pet Sci Eng* 51:223–237. <https://doi.org/10.1016/j.petro.2006.01.003>
- Cnudde V, Boone MN (2013) High-resolution X-ray computed tomography in geosciences: a review of the current technology and applications. *Earth-Sci Rev* 123:1–17. <https://doi.org/10.1016/j.earscirev.2013.04.003>
- Derluy H, Dewanckele J, Boone MN et al (2014) Crystallization of hydrated and anhydrous salts in porous limestone resolved by synchrotron X-ray microtomography. *Nucl Inst Methods Phys Res Sect B Beam Interact Mater Atoms* 324:102–112. <https://doi.org/10.1016/j.nimb.2013.08.065>
- Dierick M, Van Loo D, Masschaele B et al (2014) Recent micro-CT scanner developments at UGCT. *Nucl Inst Methods Phys Res Sect B Beam Interact Mater Atoms* 324:35–40. <https://doi.org/10.1016/j.nimb.2013.10.051>
- Dunham RJ (1962) Classification of carbonate rocks according to depositional texture. *Am Assoc Pet Geol Mem* 1:108–121
- Eberhardt E, Stead D, Stimpson B (1999) Quantifying progressive pre-peak brittle fracture damage in rock during uniaxial compression. *Int J Rock Mech Min Sci* 36:361–380. [https://doi.org/10.1016/S0148-9062\(99\)00019-4](https://doi.org/10.1016/S0148-9062(99)00019-4)
- Fronteau G, Moreau C, Thomachot-Schneider C, Barbin V (2010) Variability of some Lutetian building stones from the Paris Basin, from characterisation to conservation. *Eng Geol* 115:158–166. <https://doi.org/10.1016/j.enggeo.2009.08.001>
- Hawkins AB (1998) Aspects of rock strength. *Bull Eng Geol Environ* 57:17–30
- Hoek E, Brown ET (1980) *Underground excavations in rock*. Institution of Mining & Metallurgy
- Ji Y, Baud P, Vajdova V, Wong T -f (2012) Characterization of pore geometry of Indiana limestone in relation to mechanical compaction. *Oil Gas Sci Technol – Rev IFP Energies Nouv* 67:753–775. <https://doi.org/10.2516/ogst/2012051>
- Kahraman S (2001) Evaluation of simple methods for assessing the uniaxial compressive strength of rock. *Int J Rock Mech Min Sci* 38:981–994. [https://doi.org/10.1016/S1365-1609\(01\)00039-9](https://doi.org/10.1016/S1365-1609(01)00039-9)
- Liang CY, Zhang QB, Li X, Xin P (2016) The effect of specimen shape and strain rate on uniaxial compressive behavior of rock material. *Bull Eng Geol Environ* 75:1669–1681
- Lockner D (1993) The role of acoustic emission in the study of rock fracture. *Int J Rock Mech Min Sci Geomech Abstr* 30:883–899. [https://doi.org/10.1016/0148-9062\(93\)90041-B](https://doi.org/10.1016/0148-9062(93)90041-B)

- Makhloufi Y, Collin PY, Bergerat F et al (2013) Impact of sedimentology and diagenesis on the petrophysical properties of a tight oolitic carbonate reservoir. The case of the Oolithe Blanche formation (Bathonian, Paris Basin, France). *Mar Pet Geol* 48:323–340. <https://doi.org/10.1016/j.marpetgeo.2013.08.021>
- Masschaele BC, Cnudde V, Dierick M et al (2007) UGCT: new X-ray radiography and tomography facility. *Nucl Inst Methods Phys Res Sect A Accel Spectrometers, Detect Assoc Equip* 580:266–269. <https://doi.org/10.1016/j.nima.2007.05.099>
- Paterson MS, Wong T (2005) *Experimental rock deformation-the brittle field*. Springer Science & Business Media
- Roels S, Elsen J, Carmeliet J, Hens H (2001) Characterisation of pore structure by combining mercury porosimetry and micrography. *Mater Struct Constr* 34:76–82
- Siegesmund S, Dürrast H (2011) Physical and Mechanical Properties of Rocks. In: *Stone in Architecture - Properties, Durability*. pp 97–224
- Szwedzicki T, Shamu W (1999) The effect of discontinuities on strength of rock samples. *Proc Aust Inst Min Metall* 304:23–28
- Thuro K, Plinninger RJ, Zäh S, Schütz S (2001) Scale effects in rock strength properties. Part 1: unconfined compressive test and Brazilian test. In: Särkkä E (ed) *ISRM regional symposium Eurorock*. Espoo, Finland, pp 169–174
- Tuncay E, Hasancebi N (2009) The effect of length to diameter ratio of test specimens on the uniaxial compressive strength of rock. *Bull Eng Geol Environ* 68:491–497. <https://doi.org/10.1007/s10064-009-0227-9>
- UNE-EN 1926 (2007) NBN EN 1926:2007 Natural stone test methods - Determination of uniaxial compressive strength. *Eur Comm Stand*
- UNE-EN 1936 (2006) NBN EN 1936: Natural stone test method. Determination of Real Density and Apparent Density, and of Total and Open Porosity. *Eur Comm Stand* 3